Five centuries of reconstructed streamflow in Athabasca River Basin, Canada: Non-stationarity and teleconnection to climate patterns

Yenan Wu[1, 2], Thian Yew Gan[1], Yuntong She[1], Chongyu Xu[3], Haibin Yan[2]

[1]Department of Civil and Environmental Engineering, University of Alberta, Edmonton, Alberta, Canada.

[2]College of Hydrology and Water Resources, Hohai University, Nanjing, China

[3]Department of Geosciences, University of Oslo, Oslo, Norway

Corresponding author: Thian Yew Gan (tgan@ualberta.ca)

Key Points:

- A network of tree ring chronologies and hierarchical Bayesian model can reasonably reconstruct streamflow in Athabasca river basin
- The five centuries reconstructed streamflow show drier conditions compared to modern drought events
- The AMO index is shown to be negatively correlated with paleo streamflow data at the multidecadal time scale

Abstract

It is challenging to quantify representative long-term variability of streamflow and its possible low-frequency climate drivers from observed streamflow data available, which is usually limited. To address this issue, a hierarchical, multilevel Bayesian regression (HBR) with the partially pooled method was developed to reconstruct the 1489-2006 annual streamflow data at six Athabasca River Basin (ARB) gauging stations based on 14 tree ring chronologies. Seven nested models were developed to maximize the availability of tree ring predictors. A leave-m-out cross validation method was used to verify the model performance. The reconstruction model was demonstrated to be skillful and seems to better capture low flow than high flow scenarios. More droughts in the premeasurement proxy record with great severity and duration were found from the reconstructed data, which shows that instrumental records are deficient in representing the variability of streamflow accurately, especially at multidecadal scales. Results obtained from wavelet analysis, partial wavelet coherence, and composite analysis show the reconstructed streamflow of ARB has two statistically significant modes, one at interannual time scale (2-8 year) strongly teleconnected to ENSO and a low-frequency mode (~80 year period) which may be teleconnected to PDO and AMO. The AMO index is shown to be negatively correlated with paleo streamflow data of ARB at multidecadal time scale. The long-term streamflow reconstructions and the relationships with ENSO, PDO, and AMO provide useful information on the long-term changes in the hydrological regime of ARB.

1 Introduction

It is challenging to estimate representative natural variability of hydrological variables such as streamflow because worldwide instrumental records are limited, mostly less than 100 years, and even less than 50 years for many river basins. As a result, an exclusive reliance on limited observed data to estimate the hydrologic and climate variability of a river basin for designing its hydraulic infrastructure, reservoir operation, and water conveyance can be problematic. Geological and biological proxies collected from glaciers, sediments of lakes and marine, tree rings, and corals over the past centuries (Ho et al., 2015; Tierney et al., 2013) are viable sources of paleoclimate data that can be used to extend the instrumental records by hundreds of years during the pre-instrumental period to estimate more representative natural climate variability of the river basin. Besides short instrumental record, data collected in recent years are often affected by anthropogenic activities on our climate system (Sauchyn & Ilich, 2017). Therefore, by reconstructing the aforementioned natural proxies, to say, streamflow data, we can overcome the limitations of short gauging records (Gangopadhyay et al., 2018).

Among various proxy data available, tree ring proxy is usually preferred to reconstruct climate variables such as temperature (Borgaonkar et al., 2018), precipitation (Steinschneider et al., 2018), runoff (Ho et al., 2017), and groundwater and lake levels (Meko, 2006; Perez-Valdivia & Sauchyn, 2011), mainly because such data are widely available, and they can provide past climate characteristics at annual/sub-annual time scales (Crawford et al., 2015). Besides, tree ring signals are typically coherent within hundreds of kilometers, they provide useful hydrological signals at regional scales (Axelson et al., 2009). Tree ring based streamflow reconstructions have been applied to water resource management in Asia (Gou et al., 2010; Liu et al., 2019), America (Carson & Munroe, 2005; Patskoski et al., 2015), Europe (Wilson et al., 2005), and Africa (Gebrekirstos et al., 2014). In western Canada, tree ring proxy record has been applied to reconstruct streamflow in the Athabasca River (Bonin & Burn, 2005), Northern and Southern Saskatchewan River (Axelson et al., 2009; Sauchyn & Ilich, 2017), and Oldman River and Red Deer River basin (Elshorbagy et al., 2016; Razavi et al., 2016). The basis for reconstructing historical streamflow time series using tree ring proxy is that the climate variables such as precipitation, evapotranspiration, and temperature that control the growth of annual treewidth are related to the discharge of a nearby river (Axelson et al., 2009; Loaiciga et al., 1993; Meko et al., 1995).

Traditionally, linear or nonlinear regression models developed from tree ring data as predictors to instrumental streamflow records are applied to reconstruct streamflow of pre-instrumental periods from paleo tree ring proxy. Woodhouse (2001) used tree ring data and a stepwise regression method to reconstruct the mean annual streamflow of the Colorado Front Range. Maxwell et al. (2011) used a principal components regression (PCR) method to reconstruct the mean May-Sep streamflow of the Potomac River in the last millennium. Cook et al. (2013) also used a PCR approach to reconstruct streamflow data of the Indus River for the last 557 years. Recently, Ferrero et al. (2015) used PCR and tree ring chronology to reconstruct the first sub/tropical river streamflow in South America for the past 300 years. However, a common pitfall of traditional regression methods is that such an approach often fail to preserve multi-site correlation and uncertainties associated with reconstructed streamflow are difficult to estimate. Recently, the hierarchical Bayesian model which is more robust, and can better handle model uncertainties has been investigated in hydroclimatic applications such as regional flood frequency analysis (Wang et al., 2014), modeling of precipitation and streamflow extremes (Bracken et al., 2016; Najafi & Moradkhani, 2014), and trend detection (Sun et al., 2015). Devineni et al. (2013) used the hierarchical Bayesian regression (HBR) method to reconstruct streamflow in the upper Delaware River basin and assessed its performance with respect to multi-site information. Rao et al. (2018) used the HBR to reconstruct streamflow of three sites with short records in the Upper Indus Basin.

The Athabasca River in Alberta, Canada, the third longest unregulated river in North America, has been the source of surface water needed for extracting bitumens from oil sands (Eum et al., 2017). In recent years, new oil sands enterprises have been granted licenses and have started operation, albeit the total amounts of water withdrawn for the existing licensed projects have already exceeded the maximum water extraction capacity permitted under the water management framework Phase I of the Athabasca River (EUB, 2007). Based on historical instrumental records, most of the streamflow gauges along the Athabasca River show a decreasing trend in recent decades. Under the climate change impact, the streamflow of the Athabasca River is projected to decrease at about 8% per ^{o}C of warming (Kerkhoven & Gan, 2011). Therefore, the future streamflow of the Athabasca River may not be sufficient to meet the needs for Alberta's economic development and in-stream ecological requirements if this downward trend in streamflow continues (Alberta, 2006). The combined effect of climate change and increasing water withdrawals may threaten the water security of aboriginal people and increase the risk of water scarcity which could affect the planned mining operations. Given long-term flow records are not available for the Athabasca River, problems exist in estimating uncertainties associated with long-term streamflow projections, the non-stationarity and low-frequency oscillation of streamflow at interannual or interdecadal time scales, which would affect the oil sands development of Alberta.

The objective of this study is to reconstruct representative and credible long-term streamflow data from tree ring proxies that can help water resources engineers to estimate more accurate extreme flow events for designing more appropriate hydraulic infrastructure, and for the operation and risk management of water resources systems. This objective was achieved from applying six streamflow gauges of the Athabasca River, 14 tree ring chronologies from of 4 tree species (1489-2006 CE) to several modeling techniques: (1) A multi-level, hierarchical Bayesian model with the partially pooled method was developed to estimate the posterior probability distribution of reconstructed streamflow and model uncertainties. (2) Teleconnection of reconstructed streamflow data to large-scale climate patterns was estimated using wavelet analysis, partial wavelet coherence, and composite analysis. (3) The duration and severity of observed and reconstructed drought events are estimated and compared, to estimate representative, low frequency, past extreme droughts of the Athabasca River basin, which could not be done from limited instrumental record alone. So far, similar analysis based on pre-instrumental streamflow data, along with possible teleconnection to large-scale climate patterns in the past are mostly neglected in water resource engineering practice, even though they could have important implications to achieving effective, long-term water resource management and planning.

The manuscript is organized as follows: The study area and data are described in Section 2, methodology in Sections 3, discussions of results in Section 4, and summary and conclusions in Sections 5.

2 Study area and Data description

2.1 Study area and streamflow data

The Athabasca River Basin (ARB), with a drainage area of 159,000 km², is located between central and northern Alberta (Figure 1) and its southern margin is located in the Boreal Plain ecozone. The Athabasca River originates from the Jasper National Park and travels about 1500 miles to the Lake Athabasca. Data of six unregulated gauging sites taken from the Hydat database of Environment Canada, located on the mainstream and two tributaries of the Athabasca River, were chosen for a long-term dendrohydrological streamflow reconstruction. The detailed information of each site is shown in Table 1. The monthly October-September flow data were combined to an annual water year data because it has a better correlation with the tree ring chronology than annual data based on the calendar year. The 1914-2016 natural streamflow records for each site were found to fit a log-normal distribution well at a 0.05 significance level, but none of them have a complete record. Two sites, 07BE001 and 07BB002, have missing data from the 1930s to 1950s. The mean annual flow for most sites approximately exhibits a decreasing trend (Fig. S1). Up to 80% of the annual flow occurs in the summer, May to August. Summary statistics of flow data for each gauge are shown in Table 1. Due to a lack of updated tree ring chronology series, the actual streamflow data for calibrating the reconstruction model were taken from 1961 to 2006.

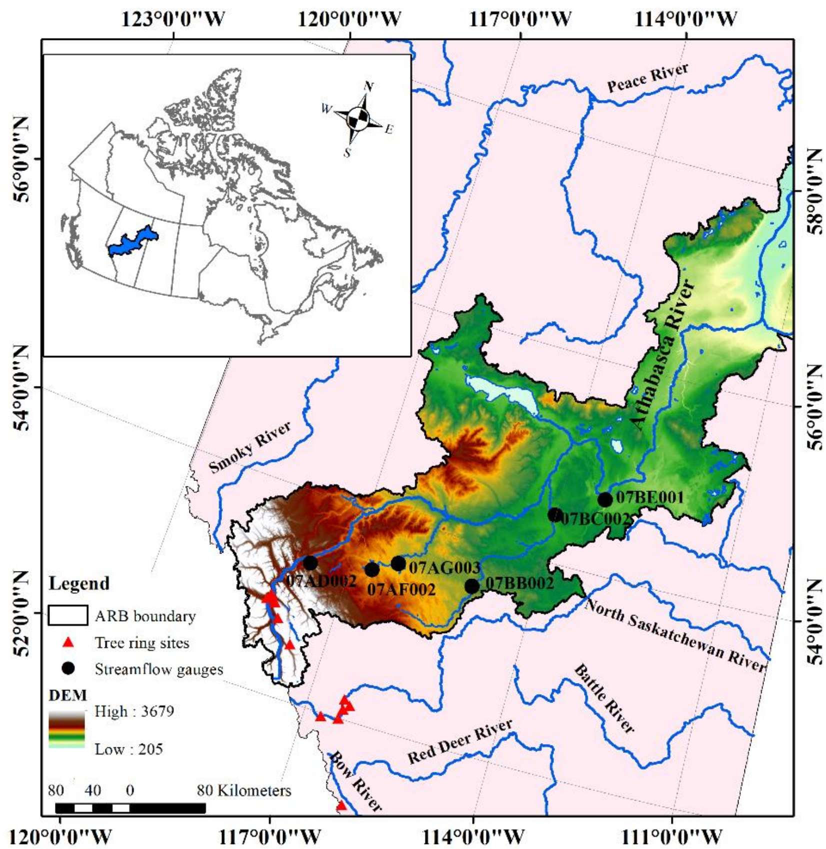

Figure 1. Location of the study area, streamflow gauges (black dots), and tree ring sites (red triangles) used in this study

Table 1. Details of streamflow gauges

Station Number	Station Name	Latitude	Longitude	Year Start	Year End	Missing Data	Annual Mean (m^3/s)	SD* (m^3/s)
07BE001	Athabasca River at Athabasca	54.72203	-113.28796	1914	2016	1931-1951	418.8	86.9
07BB002	Pembina River near Entwistle	53.60419	-115.00474	1914	2018	1924-1954	19.8	8.5
07AG003	Wolf Creek at Highway No. 16A	53.59835	-116.27184	1955	2015		3.8	1.8
07AF002	Mcleod River above Embarras River	53.47018	-116.63149	1955	2016		19.3	5.6
07BC002	Pembina River at Jarvie	54.45029	-113.99332	1961	2015		31.2	16.7
07AD002	Athabasca River at Hinton	53.42429	-117.56942	1961	2015		169.6	29.1

* SD= standard deviation.

2.2 Tree ring network

Tree ring chronologies (totally 28 sites) located in the Athabasca and the adjacent river basins that ended later than 2005 were downloaded from the International Tree-Ring Databank (https://www.ncdc.noaa.gov/data-access/paleoclimatology-data/datasets/tree-ring). The raw annual tree growth used for reconstruction is the ring width measured in millimeters per year. The ARSTAN program proposed by Cook (1985) was applied to process the tree ring data by fitting the data with a negative exponential curve or a cubic smoothing spline, a low-pass filter with a 50% frequency response cut-off for detrending and removing some non-climatic factors such as the age of trees or disturbances associated with closed canopy forests (Sauchyn et al., 2015). The annual standardized tree ring index for each chronology with different sample depth was averaged using a biweight robust function.

Appropriate tree ring predictors were selected on the basis of the Pearson correlation and the lag-one (e.g. t-1) correlation estimated between the tree ring series and six streamflow gauges. A tree ring series will be chosen as a predictor in the reconstruction model if the mean correlation coefficient between the tree ring and the streamflow is greater than 0.3 and passed the two-tailed hypothesis test at 0.05 significance level. Based on the selection criterion, 12 tree ring sites (Table S1) that contain 14 tree ring chronologies from 1062 to 2008 were used as predictors to reconstruct the streamflow of the ARB. The correlation coefficient ranges from -0.45 to 0.62 (see Figure 2). To minimize uncertainties in using tree ring chronologies to reconstruct streamflow data, the minimum number of tree ring chronologies acceptable for each year is set to be 4. As a result, 1489 is chosen as the earliest starting year. The year from 1749 to 2006 is the common period for all the tree ring sites. For several sites in the North Saskatchewan River Basin and a site U9 in the Bow River basin that located several hundred kilometers away, the tree ring data also have a significant correlation with streamflow data of ARB reflects regional climate signals. In addition, earlywood and latewood widths were considered separately for the tree ring site of Jasper Benchlands (JB8-L and JB8-E). The latewood has the highest mean correlation with the streamflow series, while the early wood was well correlated with the previous year flow records. Furthermore, given diverse tree ring species are more likely to achieve credible reconstruction results (Maxwell et al., 2011), 4 tree species (Table S1) were chosen for this study.

2.3 Climate indices

It has been demonstrated that large scale climate patterns such as El Niño Southern Oscillation (ENSO), Pacific Decadal Oscillation (PDO), and Pacific North America (PNA) are teleconnected to the hydro-climate of western North America (WNA) at interannual to inter-decadal time scales (Gan et al., 2007; Tan et al., 2016). ENSO occurs every 2~ 8 years and has a significant influence on the interannual variability of precipitation and streamflow in WNA and other parts of the world. PDO represents inter-decadal oscillations of the northern Pacific and it also modulates different phases of ENSO at interannual and multidecadal time scales. The Atlantic Multi-decadal Oscillation (AMO) has been shown to influence the streamflow variability of the upper Colorado River basin, southern United States (Erkyihun et al., 2016), and streamflow over Northern Rocky Mountain and western North American (Gray et al., 2004). Therefore, the paleo data of ENSO, PDO, and AMO were also used to explore their influence on the low-frequency oscillation and long term persistence in our reconstructed streamflow time series. The paleo reconstructions of the prior winter (November-January, NDJ) Nino 3.4 index over 1301-2005 is based on more than 2000 tree ring chronologies taken from both hemispheres (ftp://ftp.ncdc.noaa.gov/pub/data/paleo/treering/reconstructions/enso-li2013.txt). The tree-ring based paleo PDO data from 993 to 1996 was taken from the NOAA website ftp://ftp.ncdc.noaa.gov/pub/data/paleo/treering/reconstructions/pdo-macdonald2005.txt. The paleo, 1567-1990, AMO index (smoothed index of the mean SST in the North Atlantic Ocean) were derived from tree-ring based SST anomalies (ftp://ftp.ncdc.noaa.gov/pub/data/paleo/treering/reconstructions/amo-gray2004.txt) reconstructed over the North Atlantic Ocean. With a various length of records, the analysis of paleoclimate data is based on their respective overlap periods.

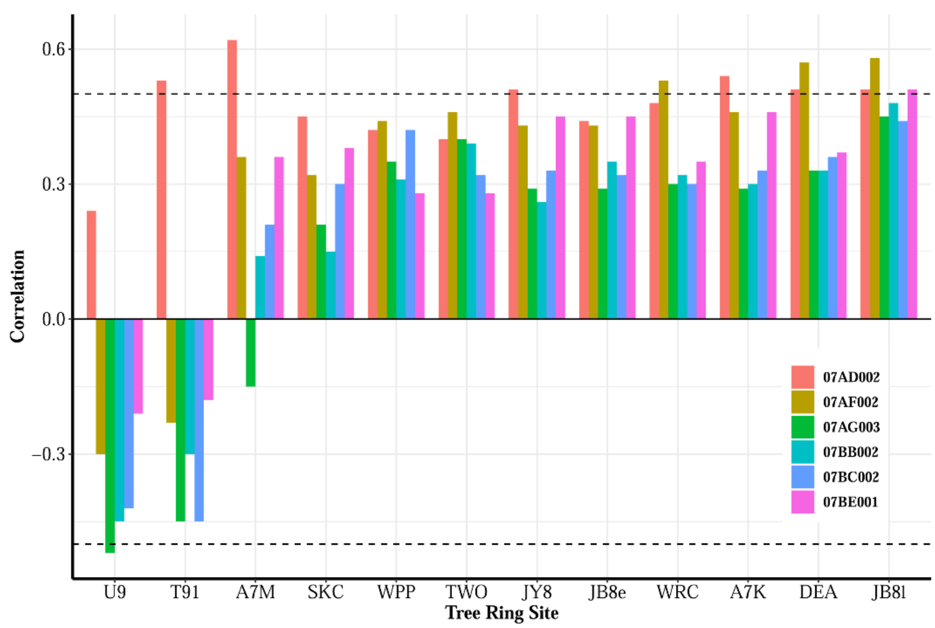

Figure 2. Pearson correlation between tree ring predictors and annual mean streamflow data of six gauging stations

3 Research Method

Regression methods are often applied with different paleoclimate data such as tree ring or sediment time series as predictors to reconstruct hydrologic variables of interest (predictands). For our study, instrumental streamflow data available across gauging sites in the boreal plains ecozone are generally short, and so it is challenging to obtain reconstructed streamflow with high credibility based on data from a single site. On the other hand, given streamflow gauges used in our study are close to each other and located in the same river basin, they are expected to come from similar physical hydrologic processes and therefore are expected to have some cross-correlation (Fig. S2). Therefore, we propose to reconstruct streamflow using a two-level, hierarchical Bayesian regression (HBR) that can incorporate multi-sites through a partially pooled method. In the first level of HBR model, regression coefficients for each streamflow gauging sites are estimated based on tree ring predictors using a linear regression method. The second level of HBR model allows the regression coefficients of each individual site may differ but are assumed to be drawn from a common multivariate normal distribution, which is the partially pooled feature of HBR. Pooling the information across all sites to an appropriate degree can effectively incorporate the regional dependency between single-site information, thus reducing the equivalent number of model parameters needed to effectively reconstruct the streamflow process and to reduce the overall uncertainties (Devineni et al., 2013b; Lima et al., 2016).

To maximize the use of available tree ring predictors, we developed a total of seven nested models with different starting year and a minimum of 20 year time steps moving backward in time (Maxwell et al., 2011), N1 (1749-2006), N2 (1693-1748), N3 (1617-1692), N4 (1576-1616), N5 (1555-1575), N6 (1534-1554), and N7 (1489-1533). The first reconstruction model N1 from 1749 to 2006 was developed using all available tree ring chronologies. The second model N2 was calibrated from 1693 to 2006 by selecting fewer long tree ring chronologies so that the full range of reconstructions can be lengthened by a period of 1693-1748, and so forth. Finally, the full range of reconstruction was extended from 1489 to 2006. In developing each nested model, Principal Component Analysis (PCA) was applied to the available tree ring predictors to obtain the first few leading principal components obtained, which together explain more than 80% of the total variance, were chosen as predictors.

Given the lack of recent tree ring and streamflow data records, we chose 1961 to 2006 as the calibration period to develop the HBR model based on the tree ring chronologies. Each nested reconstruction model was cross-validated using leave-m-out cross validation (LMOCV) method to access the performance when calibrated with different blocks of data. This approach is widely applied to a time series that are too short to be divided into calibration and validation periods. Thus, we randomly select m data from n actually used data for validation. The HBR model calibrated with the (n-m) observed data was validated against the remaining m data not used in the calibration experience. This cross-validation process is repeated p times to estimate the performance indices matrix for each model prediction. Four goodness-of-fit statistics, namely, reduction of error (RE), coefficient of efficiency (CE), peak flow criterion (PFC), and low flow criterion (LFC) were used to assess the performance of the HBR model. The RE and CE show the goodness-of-fit between reconstructed streamflow and the observations for both the calibration and validation periods, respectively. RE>0 denotes that beyond its calibration experience, HBR has some predictive ability, which tends to be higher with larger RE. CE is more stringent goodness-of-fit statistics than RE and is commonly known as the Nash-Sutcliffe coefficient (Nash

& Sutcliffe, 1970). PFC and LFC (Coulibaly et al., 2001) show the goodness-of-fit of HBR on predicted extremely high and low flow events. Smaller PFC and LFC values, closer to 0, means more representative predicted extreme peak and low flow values, respectively. Equations of goodness-of-fit statistics are given in the supplementary information (Text S1). After that, wavelet analysis, partial wavelet coherence, and composite analysis were used to explore the long term variability of reconstructed streamflow data and its teleconnection with large-scale climate patterns.

3.1 Hierarchical Bayesian regression (HBR) Model

Consider that $\log\left(Y_{i,t}\right)$ represent the log-transformed streamflow data at site *i* for year *t*. $\log\left(Y_{i,t}\right)$ can be drawn from a non-stationary normal distribution whose mean parameter can vary with time.

$$\log\left(Y_{i,t}\right) \sim N\left(\mu_{i,t}, \boldsymbol{\Sigma}\right) \tag{1}$$

The mean parameter $\mu_{i,t}$ can be estimated from a multi-linear regression model with intercepts α_i and regression coefficient matrix $\boldsymbol{\beta_i}$. where $\boldsymbol{X_t}$ is a matrix of *n* leading PCs of the tree ring series.

$$\mu_{i,t} = \alpha_i + \boldsymbol{\beta_i} * \boldsymbol{X_t} \tag{2}$$

Equations (1) and (2) represent the first level of the HBR model. The second level of the model describes the priors of parameters and hyperparameters.

$$\boldsymbol{\beta_i} \sim MVN\left(\boldsymbol{\mu_\beta}, \boldsymbol{\Sigma_\beta}\right) \tag{3}$$

$$\alpha_i \sim N\left(0, 10^4\right) \tag{4}$$

$$\boldsymbol{\mu_\beta} \sim N\left(0, 10^4\right) \tag{5}$$

$$\boldsymbol{\Sigma_\beta} \sim Inv-Wishart_{v0}\left(\Lambda_0\right) \tag{6}$$

$$\boldsymbol{\Sigma} \sim Inv-Wishart_{v1}\left(\Lambda_1\right) \tag{7}$$

We assume that the regression coefficient $\boldsymbol{\beta_i}$ (n×6) for each site are drawn from a multivariate normal distribution with a (n×1) average regression coefficient vector $\boldsymbol{\mu_\beta}$ and a (n×n) covariance matrix $\boldsymbol{\Sigma_\beta}$ that represents the correlation across the tree ring predictors. $\boldsymbol{\mu_\beta}$ and $\boldsymbol{\Sigma_\beta}$ are called hyperparameters. Non-informative prior distribution was assumed for the intercept term α_i and the hyperparameter $\boldsymbol{\mu_\beta}$. The covariance matrix $\boldsymbol{\Sigma_\beta}$ was assumed to be drawn from an inverse Wishart distribution. The setting rules for the parameter of $\boldsymbol{\Sigma_\beta}$, v_0 and Λ_0, are similar to the covariance matrix $\boldsymbol{\Sigma}$.

The (6×6) covariance matrix $\boldsymbol{\Sigma}$ is considered as a prediction error term of the multiple linear regression, its prior distribution was assumed to follow an inverse Wishart distribution with a degree of freedom parameter v_1 and a scale matrix Λ_1. The freedom parameter v_1 was set to be one more than the dimension of the matrix and the scale matrix Λ_1 was set to be an identity matrix $\boldsymbol{I}$ in the nested approach.

Thus, the whole parameters in the HBR model are $\Lambda = \left[\alpha_1, \boldsymbol{\beta_i}, \boldsymbol{\mu_\beta}, \boldsymbol{\Sigma_\beta}, \boldsymbol{\Sigma}\right]$. The posterior distribution $p\left(\Lambda|q\right)$ of the whole parameters vector for the HBR reconstruction model with the partially pooled method is described as follows:

$$p\left(\Lambda|q\right) \propto \prod_{i=1}^{I}\prod_{t=1}^{T} N\left(Y_{i,t}\left|\alpha_i + \boldsymbol{\beta_i} * \boldsymbol{X_t}, \boldsymbol{\Sigma}\right.\right) \cdot N\left(\alpha_i\left|0,10^4\right.\right) \cdot MVN\left(\boldsymbol{\beta_i}\left|\boldsymbol{\mu_\beta}, \boldsymbol{\Sigma_\beta}\right.\right) \cdot N\left(\boldsymbol{\mu_\beta}\left|0,10^4\right.\right) \cdot \\ Inv-Wishart\left(\boldsymbol{\Sigma}\left|v_1, \Lambda_1\right.\right) \cdot Inv-Wishart\left(\boldsymbol{\Sigma_\beta}\left|v_0, \Lambda_0\right.\right) \quad (8)$$

For our study, we use a Markov Chain Monte Carlo (MCMC) coupled with the Gibbs sampling method to draw values of both hyper-parameters and parameters. We randomly drew initial values for each parameter and ran three chains to verify the convergence of the results based on the Gelman–Rubin diagnostic $\hat{R}$ (Gelman & Rubin, 1992). For each chain, 10000 simulations were executed and the first 2000 simulations were discarded as a spin-up. The parameters obtained for the HBR model can be considered to have converged when the diagnostic index $\hat{R}$ is less than 1.2.

3.2 Wavelet transform analysis and partial wavelet coherence

Continuous wavelet transform (CWT) analysis and partial wavelet coherence (PWC) were used to detect statistically significant oscillations of the reconstructed streamflow and its teleconnection to paleo records of large scale climate patterns. CWT has been widely used to decompose the hydroclimatic time series for both time frequency and domain modes analyses (Li et al., 2013). CWT is also effective in detecting nonstationary signals and in identifying the variability of climate variables. More detailed information can be found in Gan et al. (2007). Global wavelet power spectrum (GWS) is used to show dominant oscillations across the scales by using an equal weight method to average the local wavelet power spectra over the study period. Since large-scale climate patterns may be interrelated with each other at different scales, the effect of other climate indices should be eliminated when estimating the coherence between a hydrologic variable and a climate index of interest, which is their partial correlation estimated by the PWC method.

4 Discussions of Results

4.1 Validity of Reconstructed Streamflow

To reconstruct the streamflow of ARB, the first three leading PCs of paleo tree ring data were retained as predictors for each nested model, except for N1 (1489-1533) with four leading PCs so that the total variance explained by the retained PCs exceeds 80%. Seven nested models based on tree ring data and the HBR were developed using 1961-2006 as the calibration period with observed streamflow data, to reconstruct the annual mean flow of 1489 to 2006 for six gauging sites of the Athabasca River. Figure 3 shows the reconstructed streamflow for site 07BE001 of the Athabasca River together with the goodness-of-fit statistics. There are 14 tree ring chronologies available from 1749 to 2006, but it gradually decreased backward in time to 4, to the earliest year of 1489. The median of the posterior distribution of reconstructed streamflow for the site 07BE001 during calibration period can explain 61.2% of the variance of instrumental records.

As can be seen from Figure 3a, the longest recent low flow period reconstructed was in 1936-1946. This happened during a period of missing data, but low Lake Athabasca water level was also reconstructed by Meko (2006) and low streamflow was observed in other river basins of Alberta (Elshorbagy et al., 2016; Sauchyn et al., 2015). This dry period could be attributed to the negative effect of the prolonged high positive PDO (St. Jacques et al., 2010). There was an abrupt transition of wet-dry-wet epochs from 1879 to 1901 also demonstrated by Sauchyn et al. (2015). The reconstructed record also shows an extremely dry event in the 1790s which was also reported by the Hudson’s Bay Company (Diaz et al., 2016; Sauchyn et al., 2015). Furthermore, reconstructed streamflow in nearby, North Saskatchewan and Red Deer River basins also show similar low flows in the 1790s (Case & MacDonald, 2003; Razavi et al., 2016). 1707 to 1730 low flow period in our reconstructions was also consistent with St. George et al. (2009) who showed a similar dry period in southern Alberta.

For assessing the performance of each nested HBR model, 10-year records were randomly selected as across validation samples. Then the cross-validation model was calibrated using the remaining 36 years of streamflow series and tree ring chronologies. This process was repeated 40 times to get an ensemble of validation metrics, of which the mean values for site 07BE001 are shown in Figure 3b. For the 1489-2006 reconstruction period, the mean RE and CE values of each nested model range from 0.35 to 0.48 and 0.27 to 0.42, respectively. As expected, both RE and CE values are the highest over the 1749-2006 period with all 14 tree ring predictors available, but deteriorate as we try to reconstruct the streamflow backward in time with correspondingly less tree ring chronologies available. Moving backward in time, the RE and CE values decrease until the year of 1693, then marginally increased going back to 1617, possibly due to the exhaustion of tree ring predictors which have relatively lower correlation coefficients with streamflow series. The statistics suggest that the reconstructed annual water year streamflow contains useful information beyond that of the calibration or validation periods. PFC and LFC are used to assess the performance of the model in reconstructing extreme conditions. Zero values in PFC and LFC mean a perfect reconstruction in peak and low streamflow values, respectively. In our study, we chose the 75 and 25 percentile of the observed streamflow data as the respective thresholds for peak and low flows. As expected, going backward in time, the mean PFC and LFC statistics of each nested model show an increasing trend, which means the ability of the model to reconstruct extreme streamflow conditions deteriorates as the number of available tree ring chronologies decreases.

PFC is generally higher than LFC for each nested model which means that the tree ring-based reconstruction models can better capture low flow than high flow variability. The high flows tend to be underestimated, partly due to other limiting environment conditions during wet years. Even with observed records during the instrumental period, the median of the posterior distribution developed for streamflow reconstructions may still underestimate the high flows such as that of 1995 and 2005.

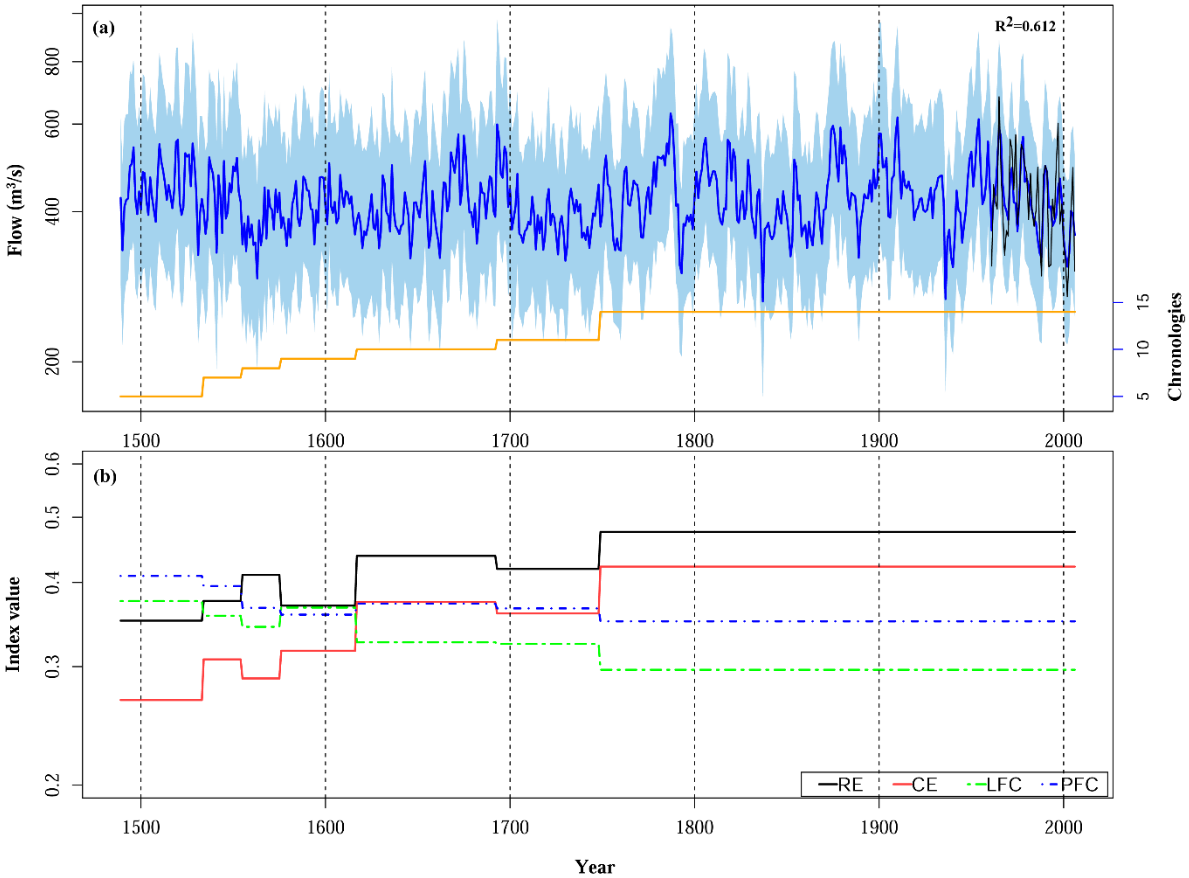

Figure 3. The reconstructed streamflow and cross-validation results for site 07BE001. (a) Blue line is the median of the posterior distribution of annual water year streamflow reconstruction and light blue region is associated 95% confidence interval from 1489 to 2006. The number of available tree ring chronologies for each nested model is plotted in yellow line while the black line shows the instrumental records. (b) The mean values of four goodness-of-fit statistics, RE (black line), CE (red line), PFC (dashed blue line), and LFC (dashed green line) for each nested model

4.2 Climate controls on streamflow

4.2.1 Wavelet spectra and coherence analysis

We extracted dominant oscillations of reconstructed streamflow for 1489-2006 at the site 07BE001. The wavelet power spectra (Fig.4a) exhibits interannual oscillations at 2~8 year scale of large amplitude during pre-1570s, 1650s-1700s, 1900s, and post-1950s, and several significant oscillations in 1780s-1870s. There are also three significant interdecadal oscillations at 16~30 year scale in 1670s-1690s, 1780s-1810s, and 1890s. The reconstructed streamflow shows a significant multidecadal component near 80-year time scale over 1690s-1940s. The significant multidecadal power at ~80 year time scale might have contributed to persistent low flows reconstructed over 1700-1950s. The GWS result shows significant low-frequency oscillations at both interannual (4~7 years) and multidecadal (~80 years) time scales. PWC was used to investigate the teleconnection between reconstructed streamflow of ARB and paleoclimate indices. Fig.4b shows the PWC between reconstructed streamflow and Nino3.4 with the influence of PDO eliminated. Apparently, most of the significant coherence occurred in 1-2 year time scale while coherence at interannual time scale (3~8 years) only occurred in 1640s-1670s, 1820s, and 1860s. There was also a strong correlation between Nino 3.4 and streamflow at the interdecadal time scale (10~14 years) between 1770s and 1840s. Fig.4c shows the PWC between the paleo PDO index and reconstructed streamflow after the influence of Nino 3.4 was eliminated. As expected, PDO generally shows scattered significant coherence with streamflow at interannual (2~8 years) and long-term multidecadal scales of 16~32 year periodicity over pre-1670s and post-1830s. PDO shows stronger coherence with reconstructed streamflow series than the Nino 3.4 index. It is noted that a significant coherence between two signals does not necessarily mean that the wavelet power of each signal is also statistically significant. For example, the significant coherence between PDO and streamflow occurred in the pre-1660s, but they did not show significant signals in their power spectrum (Fig. S3). The PWC between AMO and reconstructed streamflow (Fig.4d) shows that besides several significant coherence at interannual and interdecadal time scales, there is a persistent, significant coherence at multidecadal scales of 60~80 year periodicity from 1660s to 1950s, implying that low-frequency variations of AMO may exert a large influence on the low-frequency variability of streamflow. Enfield et al. (2001) showed that the North Pacific (mainly north of 40°N) is teleconnected to AMO through fluctuations in the tropospheric polar vortex while others showed that the northern Rocky Mountains is strongly affected by AMO and PDO (Gray et al., 2004; Hidalgo, 2004; St. Jacques et al., 2010), especially for drought events. Overall, both ENSO and PDO modulated the interannual variability of reconstructed streamflow simultaneously, while PDO had been the dominant climate pattern that affected its interdecadal variability, and AMO exerted its influence on the streamflow at multidecadal time scale. The results also show that the low-frequency variability of streamflow in ARB varies with time in the past 500 years, which demonstrates the nonstationary of climate.

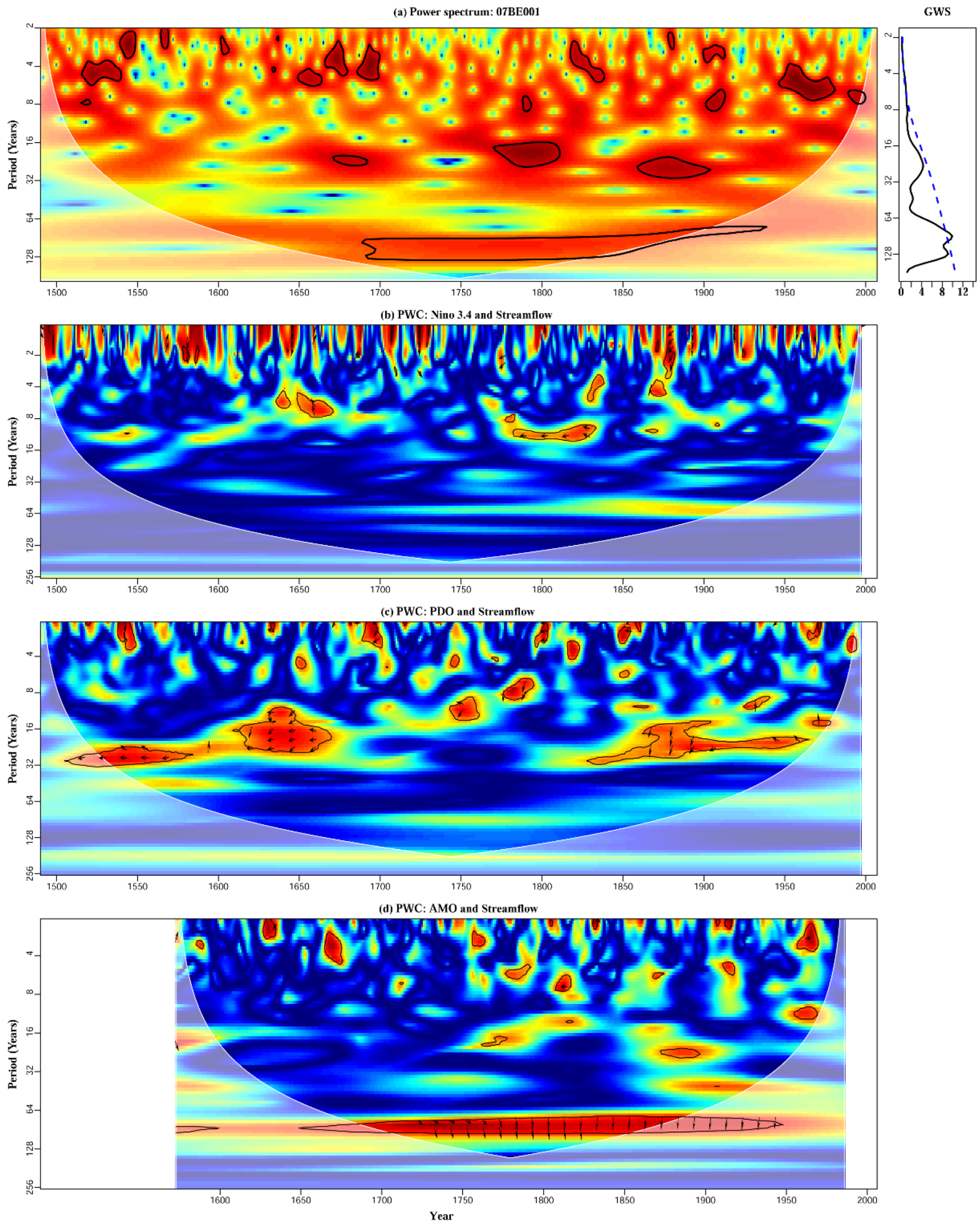

Figure 4. Wavelet analysis and partial wavelet coherence of reconstructed streamflow for site 07BE001. (a) Wavelet power spectra (left) and GWS (right) result of reconstructed streamflow from 1489 to 2006 for site 07BE001. (b-d) Partial wavelet coherence between reconstructed streamflow and Nino 3.4 (after PDO effect eliminated), PDO (after Nino 3.4 effect eliminated), and AMO (after Nino 3.4 effect eliminated). The solid black contours enclose the statistically significant coherence at a 5% significance level of a red noise process. The phase difference is shown as arrows for the coherence larger than 0.8. Arrows pointing right (left) denote the streamflow and climate signals are in phase (antiphase). Arrows pointing up (down) indicate streamflow leads climate signal by 90° (270°).

4.2.2 Correlations at multiple time scales

To better understand the teleconnection between the leading PCs of band-pass filtered signals of reconstructed streamflow and climate indices Nino3.4, PDO, and AMO, we estimated their Pearson's correlation at 1-3, 3-8, 8-30, 30-60, and 60-128 year time scales. A strong correlation at a given time scale indicates that a climate pattern has a significant influence on regional streamflow at that time scale. Pearson's correlations between the leading PCs of band-passed reconstructed streamflow and band-passed climate indices for each selected time scale are shown in Table S2. Based on Fisher's Z transform, Pearson's correlations that are statistically significant at a 5% significance level is shown in bold text. The first leading PC of each time scale explains a large percentage of the total variance, ranging from 77.7% to 88.2%. Apparently, ENSO has a relatively strong significant correlation with reconstructed streamflow at interannual time scales (1-3 and 3-8 year), while PDO's influence is more at interdecadal and multidecadal scales (8-30 and 60-128 year), and AMO's influence is mainly at 30-60 and 60-128 year time scales. AMO has relatively less influence on the annual streamflow of ARB than PDO because its influence is more limited to the summer precipitation, such as its contribution to the summer drought conditions over the central and northern Canadian Prairies (Bonsal & Shabbar, 2011; Shabbar & Skinner, 2004). On an annual basis, its overall impact is less because of its relatively weak influence on the streamflow of ARB in other seasons. Despite this, the first leading PC of the reconstructed streamflow, representing 88.2% of the total variance in the 60-128 year band, still has a significant negative correlation with the paleo AMO index (Fig.5). It seems that a strong AMO will result in less streamflow and vice versa, over 1572 to 1985, and its negative influence seems to have increased after the 1870s, but its influence was briefly positive (stronger AMO resulted in more streamflow) during 1670s-1720s.

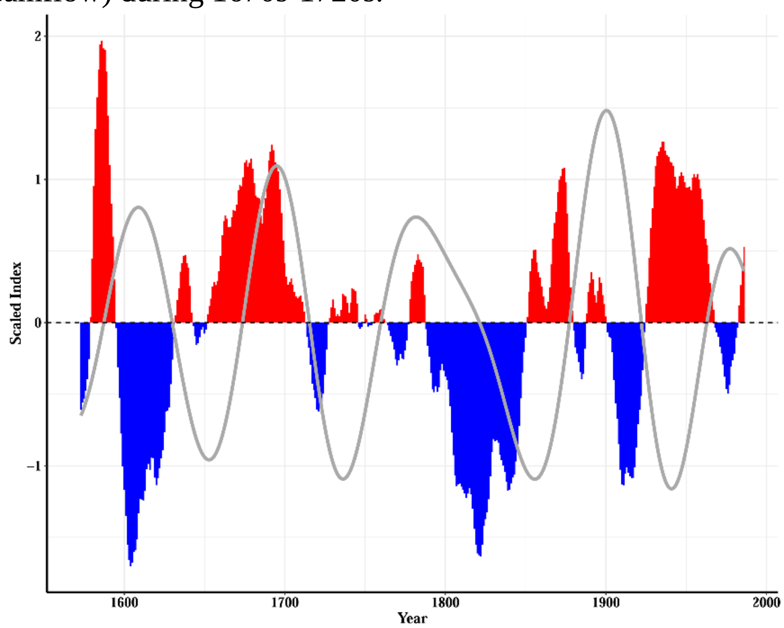

Figure 5. The low pass filtered streamflow reconstructions in 60-128 year time scale (grey line) and reconstructed climate index of AMO from Gray et al. (2004) with its positive phase shown in red and negative phase shown in blue.

4.2.3 Composite analysis

Composite analysis (Boschat et al., 2016; Welhouse et al., 2016) was used to further explore the possible influence of extreme phases of paleo ENSO, PDO, and AMO on the reconstructed annual mean streamflow across ARB. El Niño (La Niña) is considered active if the reconstructed sea surface temperature anomaly during the prior winter (November-January, NDJ) from 1489 to 2005 is above 0.5 (below -0.5). The warm (cold) phase of PDO from 1489 to 1996 and AMO from 1572 to 1985 were based on the positive (negative) paleo index value, respectively. The confidence interval for the composite streamflow of a given site was based on the ratio of the long term mean of streamflow from 1489 to 2006 for certain anomalous years by a bootstrap resampling method. Specifically, the bootstrap procedure resamples the composite streamflow associated with El Niño events to estimate the ratio of composite streamflow to the composite mean, which was repeated 500 times to obtain the distribution of composite streamflow ratios. The boxplot of composite streamflow of the six gauging sites associated with each climate pattern is shown in Fig. 6. A composite ratio value greater than 1 denotes that the climate index is associated with increased streamflow, and vice versa. Even though composite streamflow ratios vary between gauging sites, the mean composite ratios obtained from resampling 500 composite streamflow ratios under La Niña (El Niño), cold (warm) PDO, and cold (warm) AMO events are typically associated with increased (decreased) streamflow across all six streamflow gauges in ARB. The composite results for each gauge show a relatively large variance (boxplots with long whiskers), which may reflect the combined impact of two or more climate indices on the streamflow of ARB at different timescales.

To investigate the combined impact of climate patterns, we analyze streamflow anomalies in response to the interactions of ENSO-PDO, ENSO-AMO, PDO-AMO, and ENSO-PDO-AMO as shown in Fig.7. Fig.7a shows further increased (decreased) streamflow anomalies under active La Niña (El Niño) combined with cold PDO (warm PDO) regimes than streamflow under the influence of any single climate pattern. Other studies have shown that the interdecadal variations of ENSO and PDO have a synchronic influence on streamflow in western North America (Yu & Zwiers, 2007; Gan et al., 2007). Under El Niño and the cold phase of PDO, streamflow anomalies tend to be positive but generally with a large variance. The opposite effect of La Niña and warm PDO resulted in streamflow anomalies generally centered on the long term mean. The combined impact of ENSO-AMO resulted in higher (lower) streamflow when ENSO and AMO were both in phase, either cold or warm (Fig. 7b). Streamflow anomalies are negative when El Niño interacted with the cold phase of AMO is somewhat unexpected, possibly because of the asymmetrical response of ENSO to different phases of AMO (García García & Ummenhofer, 2015; Hu & Feng, 2012). The negative streamflow anomaly tends to be higher when El Niño and warm AMO occur concurrently, but the negative streamflow anomaly in response to El Niño decreases to a minimum when the effect of El Niño is offset by cold AMO. The PDO-AMO interactions in Fig.7c also show a synchronic effect on the streamflow of ARB, such that the cold (warm) phases of PDO-AMO result in enhanced positive (negative) streamflow anomalies than when either the cold (warm) phase of PDO or AMO acting alone. However, when PDO and AMO are out of phase, the effect of PDO (AMO) on the streamflow is generally suppressed by the opposite effect of AMO (PDO). As shown in Fig.7d, the driest (wettest) conditions in ARB tends to occur when El Niño (La Niña) occur together with warm (cold) PDO and warm (cold) AMO. On the other hand, when these three climate patterns were out of phase, their effects tend to cancel out each other, resulting in weak streamflow anomalies.

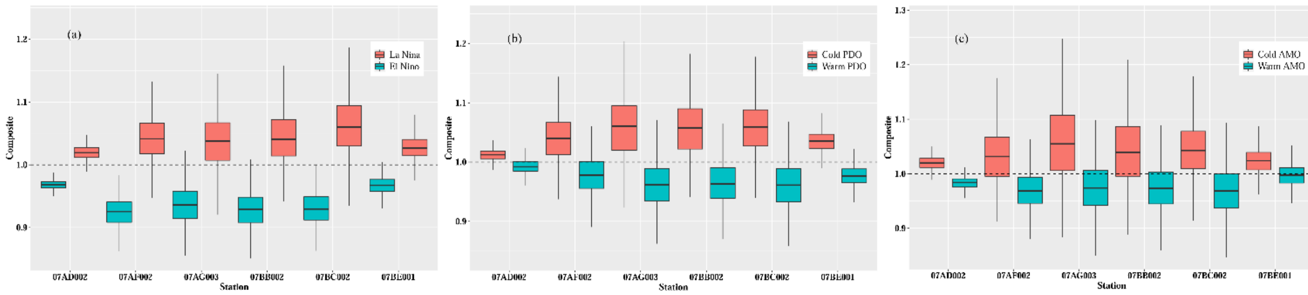

Figure 6. Composite analysis of annual reconstructed streamflow for six gauges across the ARB associated with (a) El Niño and La Niña, (b) cold and warm PDO, (c) cold and warm AMO.

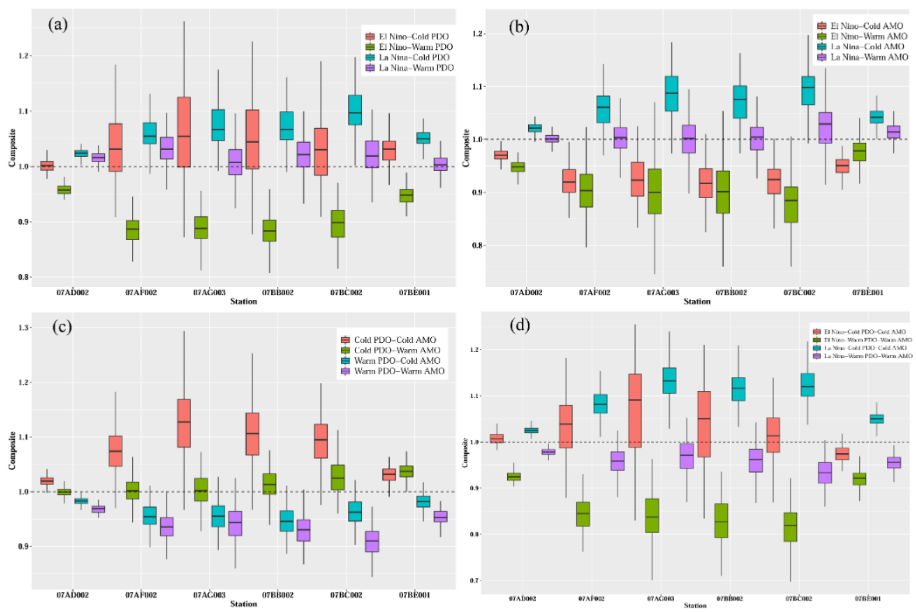

Figure 7. Composite analysis of annual reconstructed streamflow for six gauges across the ARB associated with the interactions between the different phase of (a) ENSO and PDO, (b) ENSO and AMO, (c) PDO and AMO, and (d) ENSO conditioned on PDO and AMO.

4.3 Severity and duration of dry events based on reconstructed streamflow

Given the semi-arid climate of the Canadian Prairies, prolonged droughts could affect the oilsand industries at ARB and incur severe water shortages to the agriculture and municipal sectors in southern Alberta. To gain perspective on the characteristics of droughts in the past, we use the median of posterior distributions of reconstructed streamflow series to estimate the severity and duration of the low reconstructed flow events, which would also contribute to the long-term management and sustainable, planning of the water resources of ARB with limited instrumental records. The severity of drought is defined as the departure from the long term median while the duration of drought is the duration in years below the long term median. Then 10 driest events were selected from 1-year, 5-year, 11-year and 21-year, non-overlapping running means of reconstructed streamflow, and compared with the driest events observed in instrumental records (Table 2). We used a centered, non-overlapping running mean method for a 1-year, 5-year and 11-year, and a 10-year moving window for the 21-year running means.

Based on the reconstructed streamflow series, 1837 and the 1830s-1860s period experienced the most severe individual drought event and a severe, prolonged multiyear drought event that ranked in the top ten droughts over the entire reconstruction period, respectively. Dry event of 1936 was the driest among the reconstructions for the Twentieth century, ranked the first and third in the 5 and 11-year droughts, and the tenth place in the 21-year droughts. Further, the driest instrumental event of 2002 was well replicated in the reconstructed series and ranked top among the 1-year and 5-year droughts, but the severity and duration of observed records were not among the top ten severe drought events. This shows the importance of reconstructing long-term streamflow for analyzing the long-term climate variability, especially since historical extreme drought events could occur again in modern times. The droughts of the 1560s were exceptional in terms of severity and duration, as the single and multiyear droughts were all ranked in the top five among the four running means. Our results are consistent with the 16th-century megadrought that stretched across North America into Mexico (Stahle et al., 2000). Overall, based on the median of the posterior distribution of reconstructed streamflow, the modern drought of 2002 ranks as the top 5 driest years in the last 500 years among the 1-year and 5-year running means, but less severe than the top 10 driest events at the multiyear scale.

Table 2. Top 10 driest events for the various year running means of reconstructed streamflow from 1489 to 2006 for site 07BE001 and driest events in instrumental records

Rank	**Dry events**			
	1-Year	**5-Year**	**11-Year**	**21-Year**
1	264.3 (1837)	324.3(1938)	357.0(1559)	378.3(1569)
2	267.2 (1936)	335.1(1561)	370.4(1839)	379.9(1719)
3	294.0 (1563)	348.2(2001)	373.8(1939)	386.9(1739)
4	301.0 (1793)	354.1(1986)	375.2(1714)	389.4(1859)
5	309.5(1940)	356.0(1741)	375.4(1864)	391.2(1839)
6	310.3(2002)	363.0(1621)	375.6(1624)	391.5(1629)
7	312.3(1792)	363.3(1716)	377.9(1729)	392.5(1559)
8	318.9(1730)	364.5(1861)	380.2(1744)	393.6(1649)
9	322.1(1646)	364.6(1841)	382.4(1999)	394.2(1619)
10	323.1(1662)	365.2(1661)	384.9(1644)	395.2 (1939)
Observed	270.2(2002)	331.7(2002)	387.0(2001)	398.1(1996)

5 Summary and Conclusions

In this study, we developed a hierarchical, multilevel Bayesian regression (HBR) model for reconstructing the 1489-2006 water year mean annual streamflow of the Athabasca River Basin (ARB) of Alberta using 14 tree ring chronologies and information from observed streamflow of six selected sites in the ARB. The posterior distribution for reconstructing streamflow of ARB was developed from all instrumental streamflow records of the 1961-2006 calibration period. By incorporating the multi-site information into HBR, the median results agree well with observed data and can explain more than 60% of the variance of instrumental records (Fig.4, Fig. S3). To maximize the usage of all the information of available tree ring chronologies of various length, seven nested models were developed. The cross-validation statistics RE and CE for each nested period are all positive (Fig.4, Fig. S4), demonstrating a skillful reconstruction of streamflow. Using tree ring data, reconstructing high flows was more problematic than low flows during the calibration period, as shown by higher LFC and lower PFC. Results obtained from the reconstructed streamflow of ARB are consistent with historical documents and studies on the droughts of ARB.

The wavelet spectrum and PWC of the reconstructed streamflow in ARB show two statistically significant modes, an interannual (2-8 year) and interdecadal (~80 year) time scales. The interannual variability of reconstructed streamflow had been modulated by both ENSO and PDO simultaneously, while PDO had been the dominant climate pattern that affected its interdecadal variability. From what we know, for the first time, the AMO index is shown to be negatively correlated with the streamflow of ARB at multidecadal time scale. The composite analysis shows that the La Niña (El Niño), cold (warm) PDO, and cold (warm) AMO events are typically associated with increased (decreased) streamflow anomalies across all six ARB streamflow gauges selected in this study. These climate patterns are clearly teleconnected to the streamflow of ARB, but their effects tend to cancel out each other when these climate patterns were our of phase, resulting in weaker streamflow anomalies.

The recent reconstructed droughts of the 1940s and the observed drought of 2002 rank among the top 10 most severe droughts of 1-year and 5-year durations. More droughts of greater severity with 11 and 21-year durations were found from the reconstructions, implying multidecadal variability should be considered in planning long-term strategic water policy. It seems that estimating return periods of certain events from our 518 years of reconstructed streamflow based on tree ring data will be more representative than relying on limited instrumental records. Such paleo data will also be more effective to quantify the joint probabilities of drought severity and duration using the copulas theory.

Applying HBR with partially pooled method reduces the equivalent number of model parameters, thus leads to lower reconstruction uncertainties. The HBR model developed for ARB is transferrable to other watersheds and it is flexible to incorporate other exogenous predictors than tree ring chronologies, such as ENSO climate indices as temporal covariates to forecast the nonstationarity of the variable of interest, while site characteristics such as drainage area could be used as spatial covariates. Our future research will explore the physical mechanisms behind the teleconnection of ENSO, AMO, and PDO on the streamflow of western Canada and the applications of such large-scale climate patterns to predict the long-term streamflow variability for more effective management of the water recourses.

Acknowledgments

This work was funded by Natural Science and Engineering Research Council of Canada, and the National Key R&D Program of China. The authors declare no conflicts of interest. Data set access - streamflow data: http://collaboration.cmc.ec.gc.ca/cmc/hydrometrics/www/; tree ring data: https://www.ncdc.noaa.gov/data access/paleoclimatology-data/datasets/treering.

References

Alberta. (2006). investing in our future: responding to the rapid growth of oil sands development (185).

Axelson, J. N., Sauchyn, D. J., & Barichivich, J. (2009). New reconstructions of streamflow variability in the South Saskatchewan River Basin from a network of tree ring chronologies, Alberta, Canada. *Water Resources Research*, 45(9). doi: 10.1029/2008WR007639

Bonin, D. V., & Burn, D. H. (2005). Use of tree ring reconstructed streamflows to assess drought. *Canadian Journal of Civil Engineering*, 32(6), 1114-1123. doi: 10.1139/l05-069

Bonsal, B., & Shabbar, A. (2011). Large-scale climate oscillations influencing Canada, 1900-2008 *Canadian Biodiversity: Ecosystem Status and Trends 2010, Technical Thematic Report No. 4*. Ottawa, ON: Canadian Councils of Resource Ministers.

Borgaonkar, H. P., Gandhi, N., Ram, S., & Krishnan, R. (2018). Tree-ring reconstruction of late summer temperatures in northern Sikkim (eastern Himalayas). *Palaeogeography, Palaeoclimatology, Palaeoecology*, 504, 125-135. doi: 10.1016/j.palaeo.2018.05.018

Boschat, G., Simmonds, I., Purich, A., Cowan, T., & Pezza, A. B. (2016). On the use of composite analyses to form physical hypotheses: An example from heat wave – SST associations. *Scientific Reports*, 6, 29599

Bracken, C., Rajagopalan, B., Cheng, L., Kleiber, W., & Gangopadhyay, S. (2016). Spatial Bayesian hierarchical modeling of precipitation extremes over a large domain. *Water Resources Research*, 52(8), 6643-6655. doi: 10.1002/2016WR018768

Carson, E. C., & Munroe, J. S. (2005). Tree-ring based streamflow reconstruction for Ashley Creek, northeastern Utah: implications for palaeohydrology of the southern Uinta Mountains. *The Holocene*, 15(4), 602-611. doi: 10.1191/0959683605hl835rp

Case, R. A., & MacDonald, G. M. (2003). Tree Ring Reconstructions of Streamflow for Three Canadian Prairie Rivers. *JAWRA Journal of the American Water Resources Association*, 39(3), 703-716. doi: 10.1111/j.1752-1688.2003.tb03686.x

Cook, E. R. (1985). A Time Series Analysis Approach to Tree Ring Standardization *School of Renewable Natural Resources* (PhD, pp.): University of Arizona.

Cook, E. R., Palmer, J. G., Ahmed, M., Woodhouse, C. A., Fenwick, P., Zafar, M. U.,... Khan, N. (2013). Five centuries of Upper Indus River flow from tree rings. *Journal of Hydrology*, 486, 365-375. doi: 10.1016/j.jhydrol.2013.02.004

Coulibaly, P., Bobée, B., & Anctil, F. (2001). Improving extreme hydrologic events forecasting using a new criterion for artificial neural network selection. *Hydrological Processes*, 15(8), 1533-1536. doi: 10.1002/hyp.445

Crawford, C. J., Griffin, D., & Kipfmueller, K. F. (2015). Capturing season-specific precipitation signals in the northern Rocky Mountains, USA, using earlywood and latewood tree rings. *Journal of Geophysical Research: Biogeosciences*, 120(3), 428-440. doi: 10.1002/2014JG002740

Devineni, N., Lall, U., Pederson, N., & Cook, E. (2013). A Tree-Ring-Based Reconstruction of Delaware River Basin Streamflow Using Hierarchical Bayesian Regression. *Journal of Climate*, 26(12), 4357-4374. doi: 10.1175/JCLI-D-11-00675.1

Diaz, H., Warren, J., & Hurlbert, M. (2016). *Vulnerability and Adaptation to Drought on the Canadian Prairies*: University of Calgary Press.

Elshorbagy, A., Wagener, T., Razavi, S., & Sauchyn, D. (2016). Correlation and causation in tree-ring-based reconstruction of paleohydrology in cold semiarid regions. *Water Resources Research*, 52(9), 7053-7069. doi: 10.1002/2016WR018985

Enfield, D. B., Mestas-Nuñez, A. M., & Trimble, P. J. (2001). The Atlantic Multidecadal Oscillation and its relation to rainfall and river flows in the continental U.S. *Geophysical Research Letters*, 28(10), 2077-2080. doi: 10.1029/2000GL012745

Erkyihun, S. T., Rajagopalan, B., Zagona, E., Lall, U., & Nowak, K. (2016). Wavelet-based time series bootstrap model for multidecadal streamflow simulation using climate indicators. *Water Resources Research*, 52(5), 4061-4077. doi: 10.1002/2016WR018696

EUB. (2007). Alberta Energy and Utilities Board and Government of Canada. Imperial Oil Resources Ventures Limited. Joint Panel Report. EUB Decision

Eum, H., Dibike, Y., & Prowse, T. (2017). Climate-induced alteration of hydrologic indicators in the Athabasca River Basin, Alberta, Canada. *Journal of Hydrology*, 544, 327-342. doi: https://doi.org/10.1016/j.jhydrol.2016.11.034

Ferrero, M. E., Villalba, R., De Membiela, M., Ferri Hidalgo, L., & Luckman, B. H. (2015). Tree-ring based reconstruction of Río Bermejo streamflow in subtropical South America. *Journal of Hydrology*, 525, 572-584. doi: 10.1016/j.jhydrol.2015.04.004

Gan, T. Y., Gobena, A. K., & Wang, Q. (2007). Precipitation of southwestern Canada: Wavelet, scaling, multifractal analysis, and teleconnection to climate anomalies. *Journal of Geophysical Research: Atmospheres*, 112(D10). doi: 10.1029/2006JD007157

Gangopadhyay, S., Harding, B. L., Rajagopalan, B., Lukas, J. J., & Fulp, T. J. (2009). A nonparametric approach for paleohydrologic reconstruction of annual streamflow ensembles. *Water Resources Research*, 45(6). doi: 10.1029/2008WR007201

García García, D., & Ummenhofer, C. C. (2015). Multidecadal variability of the continental precipitation annual amplitude driven by AMO and ENSO. *Geophysical Research Letters*, 42(2), 526-535. doi: 10.1002/2014GL062451

Gebrekirstos, A., Bräuning, A., Sass-Klassen, U., & Mbow, C. (2014). Opportunities and applications of dendrochronology in Africa. *Current Opinion in Environmental Sustainability*, 6, 48-53. doi: https://doi.org/10.1016/j.cosust.2013.10.011

Gelman, A., & Rubin, D. B. (1992). Inference from Iterative Simulation Using Multiple Sequences, 7(4), 457-472. doi: 10.1214/ss/1177011136

Gou, X., Deng, Y., Chen, F., Yang, M., Fang, K., Gao, L.,... Zhang, F. (2010). Tree ring based streamflow reconstruction for the Upper Yellow River over the past 1234 years. *Chinese Science Bulletin*, 55(36), 4179-4186. doi: 10.1007/s11434-010-4215-z

Gray, S. T., Graumlich, L. J., Betancourt, J. L., & Pederson, G. T. (2004). A tree-ring based reconstruction of the Atlantic Multidecadal Oscillation since 1567 A.D. *Geophysical Research Letters*, 31(12). doi: 10.1029/2004GL019932

Hidalgo, H. G. (2004). Climate precursors of multidecadal drought variability in the western United States. *Water Resources Research*, 40(12). doi: 10.1029/2004WR003350

Ho, M., Kiem, A. S., & Verdon Kidd, D. C. (2015). A paleoclimate rainfall reconstruction in the Murray‐Darling Basin (MDB), Australia: 1. Evaluation of different paleoclimate archives, rainfall networks, and reconstruction techniques. *Water Resources Research*, 51(10), 8362-8379. doi: 10.1002/2015WR017058

Ho, M., Lall, U., Sun, X., & Cook, E. R. (2017). Multiscale temporal variability and regional patterns in 555 years of conterminous U.S. streamflow. *Water Resources Research*, 53(4), 3047-3066. doi: 10.1002/2016WR019632

Hu, Q., & Feng, S. (2012). AMO- and ENSO-Driven Summertime Circulation and Precipitation Variations in North America. *Journal of Climate*, 25(19), 6477-6495. doi: 10.1175/JCLI-D-11-00520.1

Kerkhoven, E., & Gan, T. Y. (2011). Differences and sensitivities in potential hydrologic impact of climate change to regional-scale Athabasca and Fraser River basins of the leeward and windward sides of the Canadian Rocky Mountains respectively. *Climatic Change*, 106(4), 583-607. doi: 10.1007/s10584-010-9958-7

Li, M., Xia, J., Chen, Z., Meng, D., & Xu, C. (2013). Variation analysis of precipitation during past 286 years in Beijing area, China, using non-parametric test and wavelet analysis. *Hydrological Processes*, 27(20), 2934-2943. doi: 10.1002/hyp.9388

Lima, C. H. R., Lall, U., Troy, T., & Devineni, N. (2016). A hierarchical Bayesian GEV model for improving local and regional flood quantile estimates. *Journal of Hydrology*. doi: 10.1016/j.jhydrol.2016.07.042

Liu, N., Bao, G., Liu, Y., & Linderholm, H. W. (2019). Two Centuries-Long Streamflow Reconstruction Inferred from Tree Rings for the Middle Reaches of the Weihe River in Central China *Forests* (10, pp.).

Loaiciga, H. A., Haston, L., & Michaelsen, J. (1993). dendrohydrology and long-term hydrologic phenomena. *Reviews of Geophysics*, 31(2), 151-171. doi: 10.1029/93RG00056

Maxwell, R. S., Hessl, A. E., Cook, E. R., & Pederson, N. (2011). A multispecies tree ring reconstruction of Potomac River streamflow (950-2001). *Water Resources Research*, 47(5). doi: 10.1029/2010WR010019

Meko, D. M. (2006). Tree-Ring Inferences on Water-Level Fluctuations of Lake Athabasca. *Canadian Water Resources Journal*, 31(4), 229-248. doi: 10.4296/cwrj3104229

Najafi, M. R., & Moradkhani, H. (2014). A hierarchical Bayesian approach for the analysis of climate change impact on runoff extremes. *Hydrological Processes*, 28(26), 6292-6308. doi: 10.1002/hyp.10113

Nash, J. E., & Sutcliffe, J. V. (1970). River flow forecasting through conceptual models part I — A discussion of principles. *Journal of Hydrology*, 10(3), 282-290. doi: https://doi.org/10.1016/0022-1694(70)90255-6

Patskoski, J., Sankarasubramanian, A., & Wang, H. (2015). Reconstructed streamflow using SST and tree-ring chronologies over the southeastern United States. *Journal of Hydrology*, 527, 761-775. doi: https://doi.org/10.1016/j.jhydrol.2015.05.041

Perez-Valdivia, C., & Sauchyn, D. (2011). Tree-ring reconstruction of groundwater levels in Alberta, Canada: Long term hydroclimatic variability. *Dendrochronologia*, 29(1), 41-47. doi: 10.1016/j.dendro.2010.09.001

Rao, M. P., Cook, E. R., Cook, B. I., Palmer, J. G., Uriarte, M., Devineni, N.,... Wahab, M. (2018). Six Centuries of Upper Indus Basin Streamflow Variability and Its Climatic Drivers. *Water Resources Research*, 54(8), 5687-5701. doi: 10.1029/2018WR023080

Razavi, S., Elshorbagy, A., Wheater, H., & Sauchyn, D. (2016). Time scale effect and uncertainty in reconstruction of paleo-hydrology. *Hydrological Processes*, 30(13), 1985-1999. doi: 10.1002/hyp.10754

Sauchyn, D., & Ilich, N. (2017). Nine Hundred Years of Weekly Streamflows: Stochastic Downscaling of Ensemble Tree-Ring Reconstructions. *Water Resources Research*, 53(11), 9266-9283. doi: 10.1002/2017WR021585

Sauchyn, D., Vanstone, J., St. Jacques, J., & Sauchyn, R. (2015). Dendrohydrology in Canada's western interior and applications to water resource management. *Journal of Hydrology*, 529, 548-558. doi: 10.1016/j.jhydrol.2014.11.049

Sauchyn, D. J., St-Jacques, J., & Luckman, B. H. (2015). Long-term reliability of the Athabasca River (Alberta, Canada) as the water source for oil sands mining. *Proceedings of the National Academy of Sciences*, 112(41), 12621-12626. doi: 10.1073/pnas.1509726112

Shabbar, A., & Skinner, W. (2004). Summer Drought Patterns in Canada and the Relationship toGlobal Sea Surface Temperatures. *Journal of Climate*, 17(14), 2866-2880. doi: 10.1175/1520-0442(2004)017<2866:SDPICA>2.0.CO;2

St. George, S., Meko, D. M., Girardin, M., MacDonald, G. M., Nielsen, E., Pederson, G. T.,... Watson, E. (2009). The Tree-Ring Record of Drought on the Canadian Prairiesa,b. *Journal of Climate*, 22(3), 689-710. doi: 10.1175/2008JCLI2441.1

St. Jacques, J., Sauchyn, D. J., & Zhao, Y. (2010). Northern Rocky Mountain streamflow records: Global warming trends, human impacts or natural variability? *Geophysical Research Letters*, 37(6), n/a-n/a. doi: 10.1029/2009GL042045

Stahle, D. W., Cook, E. R., Cleaveland, M. K., Therrell, M. D., Meko, D. M., Grissino-Mayer, H. D.,... Luckman, B. H. (2000). Tree-ring data document 16th century megadrought over North America. *Eos, Transactions American Geophysical Union*, 81(12), 121-125. doi: 10.1029/00EO00076

Steinschneider, S., Ho, M., Williams, A. P., Cook, E. R., & Lall, U. (2018). A 500-Year Tree Ring-Based Reconstruction of Extreme Cold-Season Precipitation and Number of Atmospheric River Landfalls Across the Southwestern United States. *Geophysical Research Letters*, 45(11), 5672-5680. doi: 10.1029/2018GL078089

Sun, X., Lall, U., Merz, B., & Nguyen, V. D. (2015). Hierarchical Bayesian clustering for nonstationary flood frequency analysis: Application to trends of annual maximum flow in Germany. *WATER RESOURCES RESEARCH*, 51(8), 6586-6601. doi: 10.1002/2015WR017117

Tan, X., Gan, T. Y., & Shao, D. (2016). Wavelet analysis of precipitation extremes over Canadian ecoregions and teleconnections to large-scale climate anomalies. *Journal of Geophysical Research: Atmospheres*, 121(24), 14, 414-469, 486. doi: 10.1002/2016JD025533

Tierney, J. E., Smerdon, J. E., Anchukaitis, K. J., & Seager, R. (2013). Multidecadal variability in East African hydroclimate controlled by the Indian Ocean. *Nature*, 493(7432), 389-392. doi: 10.1038/nature11785

Wang, Z., Yan, J., & Zhang, X. (2014). Incorporating spatial dependence in regional frequency analysis. *Water Resources Research*, 50(12), 9570-9585. doi: 10.1002/2013WR014849

Welhouse, L. J., Lazzara, M. A., Keller, L. M., Tripoli, G. J., & Hitchman, M. H. (2016). Composite Analysis of the Effects of ENSO Events on Antarctica. *Journal of Climate*, 29(5), 1797-1808. doi: 10.1175/JCLI-D-15-0108.1

Wilson, R. J. S., Luckman, B. H., & Esper, J. (2005). A 500 year dendroclimatic reconstruction of spring–summer precipitation from the lower Bavarian Forest region, Germany. *International Journal of Climatology*, 25(5), 611-630. doi: 10.1002/joc.1150

Woodhouse, C. A. (2001). A Tree-Ring Reconstruction of Streamflow for The Colorado Front Range1. *JAWRA Journal of the American Water Resources Association*, 37(3), 561-569. doi: 10.1111/j.1752-1688.2001.tb05493.x

Yu, B., & Zwiers, F. W. (2007). The impact of combined ENSO and PDO on the PNA climate: a 1,000-year climate modeling study. *Climate Dynamics*, 29(7), 837-851. doi: 10.1007/s00382-007-0267-4